Optical study on doped polyaniline composite films

2004 J. Phys.: Condens. Matter 16 6195

(http://iopscience.iop.org/0953-8984/16/34/018)

INSTITUTE OF PHYSICS PUBLISHING JOURNAL OF PHYSICS: CONDENSED MATTER

J. Phys.: Condens. Matter **16** (2004) 6195–6204 PII: S0953-8984(04)80028-6

Optical study on doped polyaniline composite films

G Li[1], P Zheng[1], N L Wang[1], Y Z Long[1], Z J Chen[1], J C Li[2] and M X Wan[2]

[1] Institute of Physics and Center for Condensed Matter Physics, Chinese Academy of Sciences, PO Box 603, Beijing 100080, People's Republic of China
[2] Organic Solid Laboratory, Center for Molecular Sciences, Institute of Chemistry, Chinese Academy of Sciences, Beijing 10080, People's Republic of China

E-mail: nlwang@aphy.iphy.ac.cn

Received 27 April 2004
Published 13 August 2004
Online at stacks.iop.org/JPhysCM/16/6195
doi:10.1088/0953-8984/16/34/018

Abstract

Localization driven by disorder has a strong influence on the conducting properties of conducting polymers. Some authors hold the opinion that disorder in the material is homogeneous and that the conducting polymer is a disordered metal close to the Anderson–Mott metal–insulator (MI) transition, while others treat the disorder as inhomogeneous and have the opinion that conducting polymers are a composite of ordered metallic regions and disordered insulating regions. The morphology of conducting polymers is an important factor that has an influence on the type and extent of disorder. Different protonic acids used as dopants and moisture have influence on the polymer chain arrangement and interchain interactions. We performed optical reflectance measurements on several PANI-CSA/PANI-DBSA composite films with different dopant ratios and moisture contents. Optical conductivity and the real part of the dielectric function are calculated by Kramers–Kronig (KK) relations. $\sigma_1(\omega)$ and $\varepsilon_1(\omega)$ deviate from the simple Drude model in the low frequency range and the tendencies of the three sample are different and non-monotonic. The localization modified Drude model (LMD) in the framework of the Anderson–Mott theory cannot give a good fit to the experimental data. By introducing the distribution of relaxation time into the LMD, reasonable fits for all three samples are obtained. This result supports the inhomogeneous picture.

1. Introduction

Doped conducting polymers have been widely studied since the 1980s. Although the room temperature DC conductivity of these materials has reached that of normal metals, and some other metallic features like finite zero temperature conductivity and negative dielectric constant

are observed, the quasi-1D nature of polymer chains indicates that its conducting mechanism is different from conventional metals. Because conducting polymer samples are made up of a large number of polymer chains, the morphology of the sample has important influence on its conductivity. Disorder is usually discussed and remains controversial about whether it is homogeneous or inhomogeneous in conducting polymers [1, 2].

It is known that disorder is determined by several factors, mainly including dopants used, sample preparing procedure and later treatments. Different protonic acids used as dopants have different molecular sizes, weights and electronegativity, and thus will affect polymer chain arrangement and interchain interactions. Compared with other factors, dopants can be quantitatively controlled more easily. In this study, dopants used are camphor sulfonic acid (CSA) and dodecylbenzene sulfonic acid (DBSA). A PANI-CSA film, two PANI-CSA/PANI-DBSA composite films with different dopants ratios and an additional composite film with different moisture contents, are studied. Optical reflectivity measurements are performed on the samples. $\rho_{DC}(T)$ provides a basic understanding of conducting properties and are used to identify different transport regimes in the existence of the MI transition. However, the macroscopic T dependence of DC resistivity may not correspond to only one microscopic transport mechanism, and in conducting polymers there may exist several charge transfer processes with different timescales [3]. Reflectivity spectra, along with optical conductivity and the real part of the dielectric function calculated using KK relations, could probe the response of electron system over a large energy range and different timescales. It is an effective method for the investigation of charge transport mechanisms and several intensive studies on the reflectivity of conducting polymers exist. Although the reported reflectivity data have similar features, the analysis and explanation of the optical conductivity and the real part of the dielectric function remain controversial, especially in low frequency behaviours [4–7]. We observed different and non-monotonic tendencies in the low frequency range of the samples and tried to explain the behaviour in a unified framework.

2. Experiment

An aniline monomer is polymerized in solution in the presence of protonic acid (CSA/DBSA) as dopant, then ammonium persulfate as oxidant is dissolved in deionized water and slowly added into the previously cooled mixture. After all the oxidant is added, the reaction mixture is stirred for 24 h. The precipitate is then washed with deionized water, methanol and ethylether separately several times, and dried at room temperature in a dynamic vacuum for 24 h to finally obtain the powder of doped polyaniline. To prepare porous PANI-CSA/PANI-DBSA composite films, preparation of PANI-CSA *m*-cresol solution and preparation of PANI-DBSA chloroform solution are done separately and then the two solutions with appropriate ratio were mixed and combined with supersonic stirring. Porous films were obtained by casting the blend solution onto a glass plate. After drying at room temperature in air the polyblend was peeled off the glass substrate to form a free-standing film.

DC resistivity measurements were performed using the standard four-probe method. Copper wires were fixed on the sample films by highly conducting silver adhesive for electrical contact.

The near-normal incidence reflectance spectra were measured by using a Bruker IFS66v/S spectrometer in the frequency range from 40 to 25 000 cm^{-1}. The sample was mounted on an optically black cone in a cold-finger flow cryostat. An *in situ* overcoating technique was employed for reflectance measurements [8], which remove the effect caused by non-flatness of the sample surface. A series of light sources, beam splitters and detectors were used in different frequency ranges. The connections between different regions were excellent because

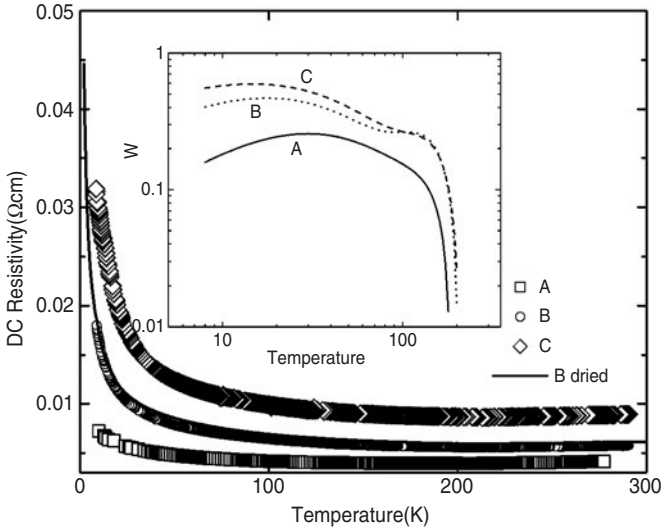

Figure 1. ρ_{DC} of samples A, B and C, from 8–300 K. B dried is the DC resistivity of sample B measured after storing in ambient air for several months, down to 2 K. There is a tiny elevation in value. The inset is the activation energy $W = \mathrm{d}(\ln\sigma)/\mathrm{d}(\ln T)$ for the three samples. $\rho_{DC}(T)$ of all samples are first fitted by six order polynomials and later calculation is based on the fitting formula; the plot range is 8–300 K.

of the identical overlap. The optical conductivity and dielectric constants were calculated by the KK relation of the reflectivity data. At the low frequency end, the Hagen–Rubens relation was used to extrapolate data towards zero as in most literature. At the high frequency end of measurement, $R(\omega)$ was extrapolated using $R \propto \omega^{-2}$ to 300 000 cm^{-1}, and beyond that a free electron behaviour of $R \propto \omega^{-4}$ was used.

3. Results and discussion

It is known from reported data that PANI-CSA is more conductive than PANI-DBSA [9, 10], because of its smaller counterion size and therefore stronger interchain interactions. We label the pure PANI-CSA film, the 15% PANI-CSA/85% PANI-DBSA blend and the 5% PANI-CSA/95% PANI-DBSA blend samples A, B, C, respectively, in the latter part of this paper. Temperature-dependent DC resistivity measurements show that $\rho_{DC}|_C > \rho_{DC}|_B > \rho_{DC}|_A$, as in figure 1. The room temperature resistivities for samples A, B, and C are 0.0042, 0.0058 and 0.0089 Ω cm, respectively. The activation energy $W = \mathrm{d}(\ln\sigma)/\mathrm{d}(\ln T)$ is used as a more effective criteria in the existence of a MI transition [11]. The slope of the plot is positive, negative and constant at low temperature for a sample in the metallic, the insulating and the critical regime, respectively. The inset of figure 1 is the W versus T plot. Sample A has a positive slope at low temperature, confirming that there are delocalized states at the Fermi level as $T \to 0$ and this sample is in the metallic region of the MI transition. The slope of samples B and C has weak T dependence, indicating that they are near the critical regime of the MI transition.

Part (a) of figure 2 is the measured reflectivity data. At the low frequency end, the sequence of reflectivity magnitude of the three samples is the same as that of their $\rho_{DC}(RoomT)$. Part (b) is the real part of $\sigma(\omega) = \sigma_1(\omega) + \imath\sigma_2(\omega)$, which is obtained through KK relations,

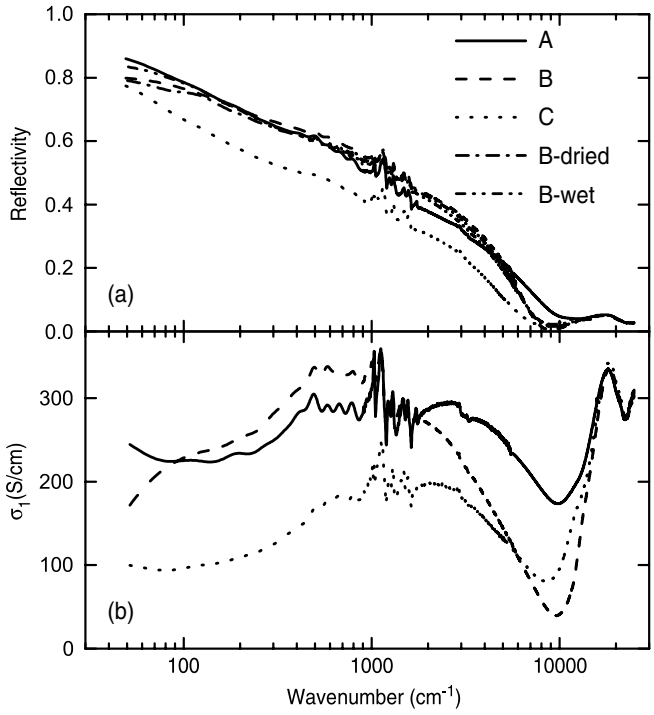

Figure 2. Part (a) is the reflectivity data for all samples, part (b) is the real part of $\sigma(\omega) = \sigma_1(\omega) + \imath\sigma_2(\omega)$ of samples A, B and C; note the difference tendency in the low frequency range.

with similar features of reported data of a series of protonic acid doped PANI and Ppy samples [4, 6, 7, 12–15]. The peak around 19 000 cm^{-1} corresponds to a π–π^* interband transition. There are a series of sharp peaks between 1000 and 1800 cm^{-1}, which are accounted for as phonon features, the peak positions corresponding to certain bond vibration modes were given in the literature elsewhere [9]. Between 1000 and 10 000 cm^{-1}, σ_1 has a Drude type behaviour. Below 1000 cm^{-1}, disregarding the phonon features, σ_1 deviates from the Drude model in that it decreases with decreasing frequency. This deviation is generally considered as an effect of localization of the electron wavefunctions. At the far IR region, $\sigma_1(\omega)$ of the three samples have different variation tendency. $\sigma_1(\omega)$ of samples A and C begin to increase below about 100 cm^{-1}, while $\sigma_1(\omega)$ of sample B continues decreasing until the low frequency edge of our measurement. This character is more obvious in linear axes. In addition, $\sigma_1(\omega)|_{\mathrm{B}}$ is larger than $\sigma_1(\omega)|_{\mathrm{A}}$ in the 100–1000 cm^{-1} range. This behaviour of optical conductivity is not consistent with $\rho_{\mathrm{DC}}(T)$, which scales with the ratio of doping protonic acids used, and suggests that the charge transport process in conducting polymers cannot be fully manifested in DC resistivity.

There is large contradiction in the reported $\varepsilon_1(\omega)$ of $\varepsilon(\omega) = \varepsilon_1(\omega) + \imath\varepsilon_2(\omega)$ derived from KK. Some authors reported a large negative value of $\varepsilon_1(\omega)$ in the far infrared range [16–18], while others reported positive $\varepsilon_1(\omega)$ in the same range [4, 14]. Due to suspicion of $\varepsilon_1(\omega)$ near the low measurement edge obtained through KK, all the authors had made efforts to ensure the effectiveness of the data. Besides affirming the reflectivity measurements, the direct dielectric measurements are used as a boundary condition [15, 19–22]. The consistency between $\sigma_1(\omega)$ and $\varepsilon_1(\omega)$ is also discussed, the results of KK should stand by causality law [23]. Figure 3 is

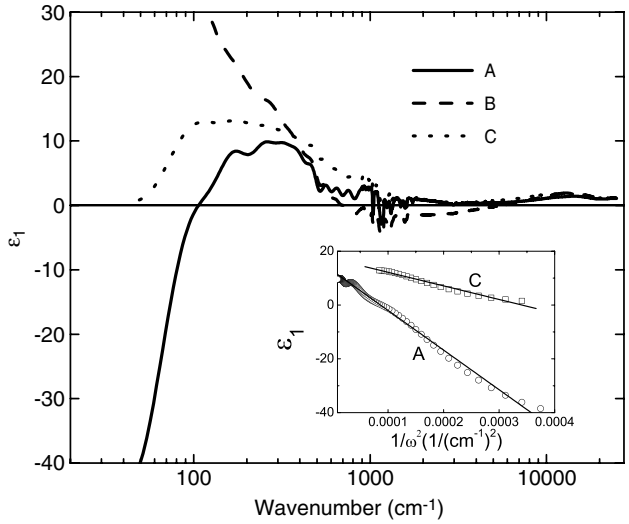

Figure 3. The real part of the dielectric function $\varepsilon(\omega) = \varepsilon_1(\omega) + \imath\varepsilon_2(\omega)$, ε_1 of samples A and C have a turnover and ε_1 of A becomes negative below 100 cm^{-1}. The inset is the ε_1 versus $1/\omega^2$ plot for samples A and C in the low frequency range. Note that a linear relationship between ε_1 and $1/\omega^2$ is a Drude type response: $\varepsilon_\omega = \varepsilon_\infty - (\omega_{p1}^2/\omega^2)$. The fitting ω_{p1} is 384 and 225 cm^{-1} for samples A and C, respectively.

our result of $\varepsilon_1(\omega)$. Features in the high frequency range are similar to reported data. In the far IR range, $\varepsilon_1(\omega)|_A$ has a turnover at approximately 300 cm^{-1} and a crossover at 106 cm^{-1}, and then becomes negative; $\varepsilon_1(\omega)|_C$ has a turnover at about 100 cm^{-1} and decreases to nearly zero at 50 cm^{-1}; $\varepsilon_1(\omega)|_B$ has no turnovers and continues to increase with decreasing frequency. Here, the low frequency behaviour shows non-monotonic change again. It is noted that changes in $\sigma_1(\omega)$ are correlated with changes in $\varepsilon_1(\omega)$. Increasing at low frequency in $\sigma_1(\omega)$ is Drude type behaviour, corresponding to negative $\varepsilon_1(\omega)$ values because the polarization of the electron systems is out of phase with the external field. Considering the background ε_∞ of conducting polymers, $\varepsilon_1(\omega)$ should decrease with decreasing frequency at low energy and become negative after a crossover. The inset of figure 3 is the $\varepsilon_1(\omega)$ versus $1/\omega^2$ plot for samples A and C in the low frequency range, confirming the existence of Drude type behaviour. We hence hold that our $\sigma_1(\omega)$ and $\varepsilon_1(\omega)$ data are reasonable.

Hopping behaviour observed in $\sigma_{DC}(T)$ [24] and deviation from the Drude model in $\sigma_1(\omega)$ and $\varepsilon_1(\omega)$ suggest that localization must be considered in conducting polymers. Because the mesoscopic morphology of samples is a tangly built up network of polymer chains, the main source of localization should be structural disorder. Whether the disorder is homogenous or inhomogeneous is still in debate. Although our $\sigma_1(\omega)$ and $\varepsilon_1(\omega)$ data have give us some hints of inhomogeneity, we still begin our fit using a homogenous model because of calculation simplicity. In the homogenous disorder model, the localization modified Drude model (LMD) in the framework of the Anderson–Mott localization theory is widely used to fit $\sigma_1(\omega)$ and $\varepsilon_1(\omega)$ [2]:

$$\sigma_{LMD}(\omega) = \frac{\omega_p^2\tau}{4\pi(1+\omega^2\tau^2)}\left[1 - \frac{C}{(k_F v_F)^2\tau^2} + \frac{C}{(k_F v_F)^2\tau^{3/2}}(3\omega)^{1/2}\right] \tag{1a}$$

$$\varepsilon_{LMD}(\omega) = \varepsilon_\infty + \frac{\omega_p^2\tau^2}{1+\omega^2\tau^2}\left[\frac{C}{(k_F v_F)^2\tau^2}\left(\sqrt{\frac{3}{\omega\tau}} - (\sqrt{6}-1)\right) - 1\right] \tag{1b}$$

where ω_p is the plasma frequency, k_F the Fermi wavevector, v_F the Fermi velocity, τ the relax-

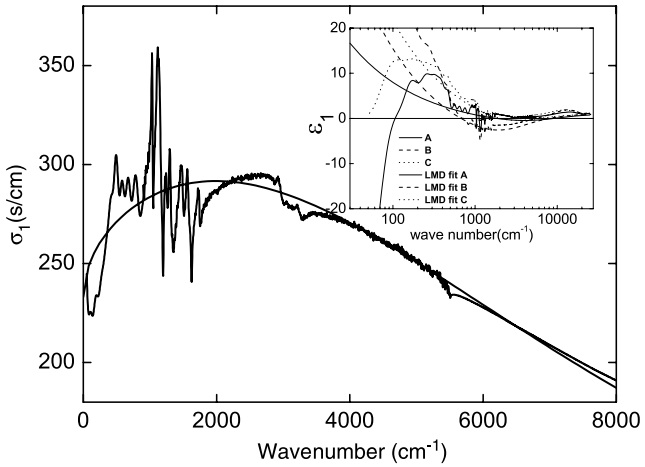

Figure 4. The LMD model fit of sample A, in the range 50–8000 cm^{-1}. The inset is a comparison of $\varepsilon_1(\omega)$ given by the LMD model using the same parameters of $\sigma_1(\omega)$ fit and experimental data. For samples A and C, the fitting curve and experimental data have opposite behaviours in the low frequency range.

Table 1. Fitting parameters of the LMD model; $\sigma_1(0)$ is the calculated zero frequency optical conductivity. Note that they are not in good accordance with room temperature σ_{DC}. $k_{\mathrm{F}}\lambda$ is calculated by $k_{\mathrm{F}}v_{\mathrm{F}} \times \tau$.

Sample	ω_{p} (cm^{-1})	$1/\tau$ (cm^{-1})	$C/(k_{\mathrm{F}}v_{\mathrm{F}})^2$ (s^2)	$\sigma_1(0)$ (S cm^{-1})	$\sigma_{\mathrm{DC}}(RT)$ (S cm^{-1})	$k_{\mathrm{F}}\lambda$
A	12 185	1/0.000 13	$1.31\mathrm{e}^{-31}$	233	241	1.91
B	7 976	1/0.000 33	$1.17\mathrm{e}^{-30}$	216	174	1.62
C	6 823	1/0.000 28	$1.65\mathrm{e}^{-30}$	55	110	1.16

ation time, ε_∞ the high energy dielectric constant, and C a universal constant ($\sim$1). Figure 4 is the plot of $\sigma_1(\omega)|_{\mathrm{A}}$ and its LMD fit, ranging from 50 to 1000 cm^{-1}. Disregarding the phonon features, the LMD model gives a good fit to the experimental data except in the low frequency range. The fitting parameters and deduced values for samples are in table 1.

The order parameter $k_{\mathrm{F}}\lambda$ for three samples are all close to the Ioffe–Regel criterion $k_{\mathrm{F}}\lambda \sim 1$, indicating that these samples are close to a MI transition according to the activation energy $W = \mathrm{d}(\ln\sigma)/\mathrm{d}(\ln T)$ plot. The values of τ have a magnitude of 10^{-15} s, as in previous studies. However, there is some erratic behaviour in $\sigma_1(\omega)$ which could not be satisfactorily explained. Sample A of the largest $\sigma_{\mathrm{DC}}(RoomT)$ has the shortest relaxation time. Relaxation time is a reflection of the extent of disorder of the material. Whether this fact accounts for the non-monotonic variation of $\sigma_1(\omega)$ in the far IR is not clear. The increasing tendency of $\sigma_1(\omega)$ of samples A and C in the low energy end could not be fitted by LMD using these parameters either. The inset of figure 4 is the plot of $\varepsilon_1(\omega)$ with the LMD fit, using the same parameters from the $\sigma_1(\omega)$ fit. It is clear that $\varepsilon_1(\omega)$ of the LMD could not simulate the decreasing tendency at low frequency of samples A and C. In the LMD model, the low frequency $\sigma_1(\omega)$ is suppressed due to localization, and $\varepsilon_1(\omega)$ becomes positive because disorder scattering reduces the relaxation time. Although there is a good fit for sample B in both $\sigma_1(\omega)$ and $\varepsilon_1(\omega)$, the Drude type behaviour of samples A and C at low frequency indicates that the LMD model is not fully applicable in the present study. Inhomogeneity in the samples must be considered.

Table 2. Fitting parameters of the LMD model with a distribution of relaxation time τ; Δ is the expansion of relaxation time.

Sample	ω_p (cm^{-1})	$1/\tau_0$ (cm^{-1})	$C/(k_F v_F)^2$ (s^2)	$1/\Delta$ (cm^{-1})	$\sigma_1(0)$ (S cm^{-1})
A	10 900	1/0.000 15	4.50e^{-31}	1/0.000 017	328
B	7 880	1/0.000 31	1.18e^{-30}	1/0.000 000 27	180
C	6 500	1/0.000 27	2.17e^{-30}	1/0.000 037	177

In an inhomogeneous picture, conducting polymers are treated as composite materials containing mesoscopic ordered regions and amorphous regions. In the ordered regions, polymer chains have good alignment and thus good interchain overlapping. Electrons in these regions are delocalized and show metallic behaviour. In the disordered regions, quasi-one dimensional localization plays the dominant role because of the quasi-one dimensional nature of a single polymer chain. In this picture, the Drude type response in $\sigma_1(\omega)$ and $\varepsilon_1(\omega)$ in the low far-IR range is explained by a small fractions of delocalized charge carriers with very long relaxation time $\sim 10^{-13}$ s, as indicated by a very small plasma frequency in $\varepsilon_1(\omega)$, while the majority of carriers are localized. It is clear that movement of electrons within a ordered region, between ordered regions and in disordered regions have different mechanisms and characteristic timescales, so it is difficult to describe the energy dependence of the response by a uniform formula over a wide frequency range. Considering that the general feature of $\sigma_1(\omega)$ at high frequency can be fitted by both a homogeneous model or an inhomogeneous model [22], we followed [1] using a distribution function of relaxation time τ to introduce inhomogeneity into the LMD model. τ of most part of carriers has a magnitude of 10^{-15} as a Ioffe–Regel criterion $k_F\lambda \sim 1$ allowed, while a small fraction of carriers has a long τ as experimentally observed. $\sigma_1(\omega)$ and $\varepsilon_1(\omega)$ are given as:

$$\sigma_{\text{inhomo}}(\omega) = \int_0^\infty P(\tau)\sigma_{\text{LMD}}(\omega, \tau)\,\mathrm{d}\tau \tag{2a}$$

$$\varepsilon_{\text{inhomo}}(\omega) = \int_0^\infty P(\tau)\varepsilon_{\text{LMD}}(\omega, \tau)\,\mathrm{d}\tau \tag{2b}$$

where $P(\tau)$ is the distribution function of relaxation time.

$$P(\tau) = \frac{2\Delta}{\pi}\left[\frac{\tau^2}{(\tau^2 - \tau_0^2)^2 + \tau^2\Delta^2}\right] \tag{3}$$

where τ_0 is the average relaxation time, Δ is the expansion of relaxation time. Figure 5 is the $\sigma_1(\omega)$ and $\varepsilon_1(\omega)$ fit for samples A, B and C; fitting parameters are in table 2.

Behaviours in the low frequency range for the three samples are all qualitatively simulated by including the distribution function of τ. The ratio Δ/τ_0 for samples A and C $\sim$0.1, while that for sample B $\sim$0.001. As an estimation, integration of τ from $0.5 \times 10^2\tau_0$ to $5 \times 10^2\tau_0$ would give the fraction of carrier concentration whose relaxation time has the magnitude 10^{-13} s, the results are 0.001 for samples A and C, and 0.0001 for sample B. Another estimation of the fraction, is to compare the small plasma frequency ω_{p1} derived from the low frequency ε_ω versus $1/\omega^2$ plot in the inset of figure 3 and the plasma frequency ω_p from the LMD fit, as done in [17]:

$$\delta = (m_1^*/m^*)(\omega_{p1}/\omega_p)^2. \tag{4}$$

The results are 0.000 99 and 0.0011 for samples A and C, respectively. Although ω_{p1} derived from such a small frequency range and the assumption that $m_1^* \sim m^*$ are doubtful, we still see

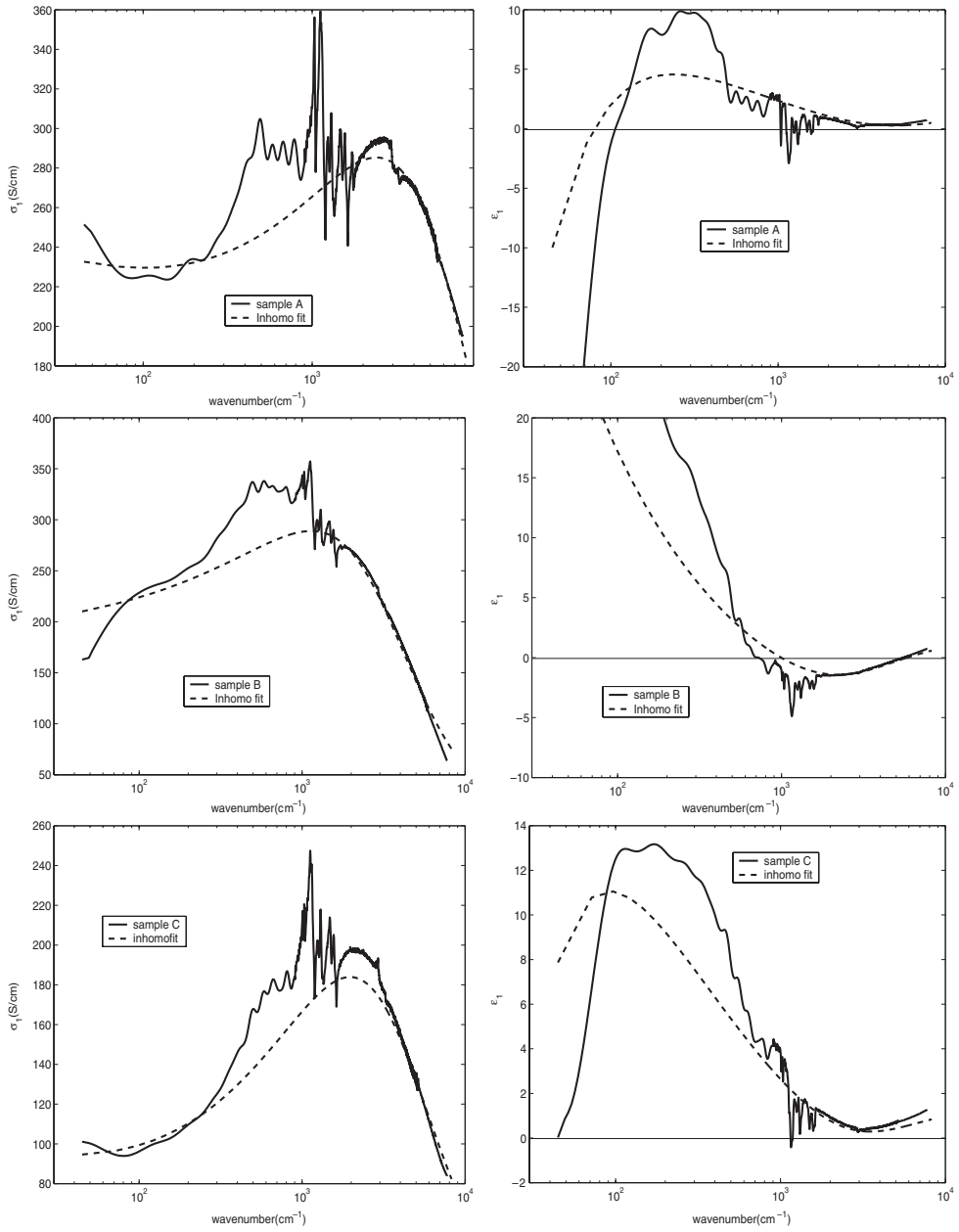

Figure 5. Fits of the LMD model with a distribution of relaxation time. The Drude type behaviour of samples A and C in the low frequency range are roughly simulated. There is also a qualitatively good fit for sample B.

that the two estimations give the same results, indicating that there are more carriers with long relaxation times existing in samples A and C, and an increase in Δ will induce a turnover from positive ε_1 to negative.

Although sample B has the largest average τ_0, the tiny expansion indicates that τ of most of its carriers have the scale 10^{-15} as the Ioffe–Regel criterion predicted, so the localization effect

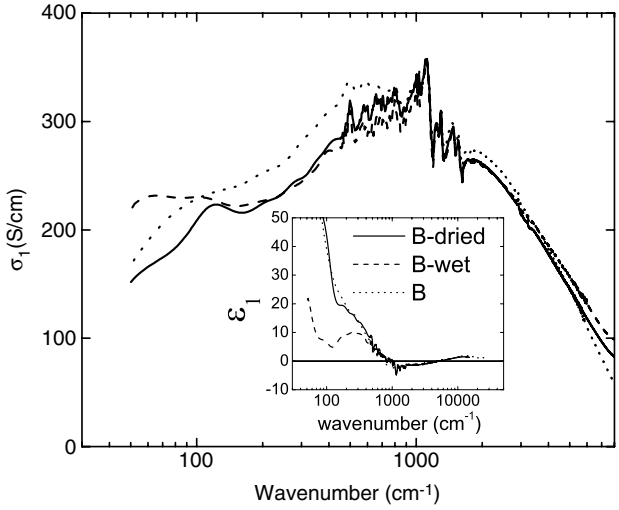

Figure 6. Optical conductivity of sample B and its dried and moistened form; the inset is their $\varepsilon_1(\omega)$ plot.

is dominant in sample B while samples A and C have a fraction of carriers showing behaviour of delocalized electrons. This non-monotonicity results from the difference in the extent of disorder, or the intensity of intra and interchain interactions, which is not entirely determined by the composition of the samples. The presence of moisture has been observed to affect the DC conductivity of conducting polymers significantly [25], and the moisture influence on sample quality should be manifested in optical data. Reflectivity measurements are performed on two samples which have the same composition as sample B, one is stored in ambient air for over 12 months (B-dried), whose DC resistivity data are show in figure 1, and the other is also stored but damped with water just before measurements (B-wet). Figure 6 shows the optical conductivity for sample B, B-dried and B-wet. $\sigma_1(\omega)$ of B-dried is lower than B in far-IR range, with similar tendency, while that of B-wet is larger than B below 100 cm^{-1}. It is assumed that removal of water molecules will reduce the structural order between polymer chains in the metallic regions as well as on chains bridging the metallic regions, in an inhomogeneous picture [26], so the increase in low frequency $\sigma_1(\omega)$ of B-wet can be interpreted as an enhancement of the tunnelling between metallic regions in low frequency [3] due to reduced potential barriers, as water molecules could reduce the polarization effects of the counteranion, and hence decrease the scattering cross section due to the counteranions. A fit to B-wet as done in last paragraph gives $\omega_\mathrm{p} = 8500\ \mathrm{cm}^{-1}$, $1/\tau_0 = 0.000\,24\ \mathrm{cm}^{-1}$, $C/(k_\mathrm{F}v_\mathrm{F})^2 = 5.9\mathrm{e}^{-31}\ \mathrm{s}^2$, $1/\Delta = 0.000\,008\ \mathrm{cm}^{-1}$. The ratio $\Delta/\tau_0 \approx 0.03$, obviously larger than that of B, indicating that in the wet sample the concentration of carriers with a long τ increases. However, $\sigma_1(\omega)$ of B-wet is lower than B in 200–1000 cm^{-1}, almost the same as B-dried, its $\varepsilon_1(\omega)$ (inset of figure 6) is lower than B and B-dried but is still positive with two turnovers. This suggests that the increase in tunnelling rate between grains cannot compensate for the general increase of disorder, and according to the conclusion that low frequency behaviour is determined by the competition between coherent and incoherent channels [22].

4. Conclusion

Absolute reflectivity measurements are performed on one PANI-CSA film, two PANI-CSA/PANI-DBSA composite films and an additional composite film with different moisture

contents. Variation of the counter-ion composition and moisture content is supposed to modulate the polymer chain arrangement and interactions. The charge transport process in conducting polymers cannot be fully manifested in DC resistivity. The optical conductivity and the real part of the dielectric function are calculated through Kramers–Kronig relations and the validity of the data is discussed. $\sigma_1(\omega)$ and $\varepsilon_1(\omega)$ derived from a simple Drude model in low frequency range and tendencies of the samples are different and non-monotonic. The localization modified Drude model in the framework of homogeneous disorder cannot explain the behaviour of the two samples. After considering the inhomogeneity by inducing a distribution function of the relaxation time into the LMD model, $\sigma_1(\omega)$ and $\varepsilon_1(\omega)$ of the samples are all qualitatively well fitted and explained. This result supports the picture that disorder in the samples is inhomogeneous and the samples consist of ordered metallic regions and disordered regions.

Acknowledgments

This work is supported by the National Science Foundation of China (Grant No. 10025418) and the Knowledge Innovation Project of the Chinese Academy of Sciences.

References

[1] Kohlman R S and Epstein A J 1998 *Handbook of Conducting Polymers* 2nd edn, vol 3 (New York: Dekker)
[2] Menon R, Yoon C O, Moses D and Heeger A J 1998 *Handbook of Conducting Polymers* 2nd edn, vol 2 (New York: Dekker)
[3] Prigodin V N and Epstein A J 2002 *Synth. Met.* **125** 43
[4] Lee K, Heeger A J and Cao Y 1993 *Phys. Rev.* B **48** 14884
[5] Kohlman R S, Tanner D B, Ihas G G, Min Y G, MacDiarmid A G and Epstein A J 1997 *Synth. Met.* **84** 709
[6] Tzamalis G, Zaidi N A, Homes C C and Monkman A P 2002 *Phys. Rev.* B **66** 085202
[7] Chapman B, Buckley R G, Kemp N T, Kaiser A B, Beaglehole D and Trodahl H J 1999 *Phys. Rev.* B **60** 13479
[8] Homes C C, Reedyk M, Crandles D A and Timusk T 1993 *Appl. Opt.* **32** 2973
[9] Lu X H, Ng H Y, Xu J W and He C B 2002 *Synth. Met.* **128** 167
[10] Long Y Z, Chen Z J, Wang N L, Zhang Z M and Wan M X 2003 *Physica* B **325** 208
[11] Menon R, Yoon C O, Moses D and Heeger A J 1993 *Phys. Rev.* B **48** 17685
[12] Tzamalis G, Zaidi N A, Homes C C and Monkman A P 2001 *J. Phys.: Condens. Matter* **13** 6297
[13] Lee K, Reghu M, Yuh E L, Sariciftci N S and Heeger A J 1995 *Synth. Met.* **68** 287
[14] Lee K, Menon R, Yoon C O and Heeger A J 1995 *Phys. Rev.* B **52** 4779
[15] Lee K and Heeger A J 2003 *Phys. Rev.* B **68** 035201
[16] Kohlman R S, Joo J, Wang Y Z, Pouget J P, Kaneko H, Ishiguro T and Epstein A J 1995 *Phys. Rev. Lett.* **74** 773
[17] Kohlman R S, Joo J, Min Y G, MacDiarmid A G and Epstein A J 1996 *Phys. Rev. Lett.* **77** 2766
[18] Kohlman R S, Zibold A, Tanner D B, Ihas G G, Ishiguro T, Min Y G, MacDiarmid A G and Epstein A J 1997 *Phys. Rev. Lett.* **78** 3915
[19] Joo J, Oblakowaki Z, Du G, Pouget J P, Oh E J, Wiesinger J M, Min Y, MacDiarmid A G and Epstein A J 1994 *Phys. Rev.* B **49** 2977
[20] Martens H C F, Reedijk J A, Brom H B, de Leeuw D M and Menon R 2001 *Phys. Rev.* B **63** 073203
[21] Martens H C F, Brom H B and Menon R 2001 *Phys. Rev.* B **64** 201102
[22] Romijin I G, Hupkes H J, Martens H C F, Brom H B, Mukherjee A K and Menon R 2003 *Phys. Rev. Lett.* **90** 176602
[23] Kittel C 1976 *Introduction to Solid State Physics* (New York: Wiley)
[24] Zuppiroli L, Bussac M N, Paschen S, Chauvet O and Forro L 1994 *Phys. Rev.* B **50** 5196
[25] Kahol P K, Dyakonov A J and McCormick B J 1997 *Synth. Met.* **89** 17
[26] Pinto N J, Shah P D, Kahol P K and McCormick B J 1996 *Phys. Rev.* B **53** 10690